Croatian Society for Materials Protection

Metalurgija/Metallurgy

Vol. 66 No. 1 / 2027

Study of Aging Time of Manganese-Copper Damping Alloy on the Reverberation Time of Piano Room Sound

Bin Sun [1,*]

https://doi.org/10.64486/m.66.1.11

[1] School of Music and Dance, Harbin University, Harbin, Heilongjiang, China
* Correspondence: 15104629776@163.com; Tel.: +8615104629776

Type of the Paper: Article
Received: March 3, 2026
Accepted: July 6, 2026

Abstract: This study investigates the effect of aging time on the microstructure, damping properties, and acoustic performance of CuMn50 manganese–copper damping alloy used as vibration-damping lining material in piano rooms. Samples were solution treated and aged for different durations, followed by microstructural characterization using XRD, SEM, and EDS, damping evaluation by DMA, and reverberation time measurements. The results show that aging time significantly affects spinodal decomposition, microstructural evolution, and damping behavior. Under the investigated experimental conditions, an aging time of 8 h produced the most favorable combination of microstructure and damping performance, resulting in the shortest reverberation time. Excessively short aging resulted in incomplete phase decomposition, whereas prolonged aging caused grain coarsening and α-Mn precipitation, reducing damping performance. Statistical analysis confirmed significant differences among the aging conditions. The findings provide a basis for further optimization of the heat treatment of manganese–copper damping alloys intended for acoustic vibration-control applications.

Keywords: manganese-copper damping alloy; aging time; microstructure evolution; damping properties; room acoustics; reverberation time

1. Introduction

The indoor acoustic environment of a professional piano room is the core foundation for vocal music training, piano performance and audio recording, with reverberation time serving as the key quantitative indicator for evaluating the acoustic performance of the piano room. The optimal range of reverberation time in the core auditory frequency band of 250–4000 Hz for professional piano rooms is (0.3–0.5) s. The multiple reflections and energy superposition of sound waves on the indoor enclosure surfaces of the piano room are the primary causes of excessive reverberation time and acoustic defects. In this study, high-damping manganese-copper alloy is designed and used as a damping vibration attenuation lining material for the inner surfaces of piano room walls and floors, rather than a structural component of the piano body (such as piano soundboard) or porous acoustic absorption material. The core functional mechanism of the alloy lining is to dissipate the vibration energy excited by incident sound waves through the inherent high damping characteristics of the material, suppress the secondary radiation of sound waves from the enclosure structure, reduce the repeated reflection of sound waves in the room, and thus achieve precise control of the indoor reverberation time.

Manganese-copper alloy is a typical strain-induced thermoelastic martensitic high-damping alloy. Its inherent damping performance stems from the stress-induced sluggish movement of twin boundaries at the parent phase–martensite (γ–M) interface, and heat treatment is the core means to regulate its microstructure and inherent damping performance [1–5]. Stress-induced aging, as a post-treatment process for manganese-copper alloys after solid solution, achieves the re-precipitation of the γ' phase from the γ solid solution by means of low-temperature insulation, enabling the formation of Mn-rich twin boundaries with an orderly arrangement of Mn atoms, thereby constructing a large number of movable phase interfaces and enhancing the damping performance of the alloy [6–10]. For CuMn50 alloy, the aging temperature is the core prerequisite for determining the thermodynamic feasibility of spinodal decomposition and the rate of atomic diffusion. Existing studies have confirmed that the effective spinodal decomposition temperature range of Mn-Cu alloys with 50 wt.% Mn content is concentrated in (380–450) °C; below this range, the diffusion rate of Mn atoms is too slow to achieve effective element segregation and phase decomposition within a conventional aging cycle, while above this range, excessive atomic diffusion activity will lead to rapid grain coarsening and premature precipitation of brittle α-Mn phase, which is not conducive to the regulation of damping performance [9,20].The aging time directly determines the adequacy of atomic diffusion and phase decomposition. An excessively short aging time leads to incomplete phase decomposition and a reduction in the number of twin-rich regions; conversely, an excessively long aging time can easily trigger grain coarsening and second-phase precipitation, thereby reducing the phase interface activity [11–14]. Existing studies have mostly focused on the effects of isothermal aging [15–16], solid solution processes [17-18], and thermomechanical treatment on the damping performance of manganese-copper alloys[19-20], but there are few systematic reports on the single-factor influence of aging time (4 h, 8 h, 12 h, 16 h) on microstructural evolution, damping performance regulation, and the quantitative correlation between alloy damping performance (as room acoustic lining) and piano room reverberation time.

In this paper, rolled CuMn50 manganese-copper alloy is used as the research object to conduct a single-factor aging time test. By fixing the solid solution temperature and process, the effects of aging time (4 h, 8 h, 12 h, 16 h) on the alloy's phase composition, micro-morphology, and elemental distribution are systematically studied, revealing the regulation mechanism of aging time on the alloy's damping performance. Combined with the actual acoustic test in a standard piano room with a clear installation scheme of the alloy lining, complete boundary conditions, a blank control group without any acoustic treatment (initial state of the room) and a conventional polyester fiber acoustic panel control group, a quantitative relationship between aging time and reverberation time is established, the actual acoustic contribution of the manganese-copper alloy lining relative to the initial room state is quantitatively characterized, and the most favorable aging process for manganese-copper alloy for piano acoustic vibration reduction is determined, with complete statistical analysis of all test data to ensure the reliability of the conclusion, providing a theoretical basis for subsequent engineering application research, rather than directly applicable engineering parameters.

2. Experimental Section

2.1. Experimental Materials

The experimental material was industrial rolled CuMn50 manganese-copper alloy sheet with a thickness of 5 mm. After wire cutting into standard test samples, the chemical composition was quantitatively analyzed by an X-ray energy dispersive spectrometer (EDS), and the results are shown in Table 1. The original mechanical properties of the alloy are as follows: tensile strength R_m = 596.7 MPa, yield strength $R_{0.2}$ = 366.7 MPa, elongation A = 30.3 %, which are consistent with the conventional mechanical properties of rolled manganese-copper alloy.

Table 1. Chemical composition of CuMn50 manganese-copper alloy (wt.%)

Mn	Cu	Al	Ni	Fe	Other impurities
49.8–50.2	Balance	0.5–0.8	0.3–0.5	0.7	≤0.1

https://doi.org/10.64486/m.66.1.11

2.2. Experimental Process

A single-factor experiment was adopted, with aging time as the only variable, and the solution treatment process, aging temperature and cooling method were fixed. The aging temperature was fixed at 420 °C, and the selection basis of this temperature is as follows: (1) Thermodynamic matching: 420 °C is located in the optimal thermodynamic window for spinodal decomposition of CuMn50 alloy, which can ensure the continuous and sufficient spinodal decomposition of supersaturated γ solid solution, and avoid the inhibition of atomic diffusion caused by too low temperature or the abnormal grain growth and harmful phase precipitation caused by too high temperature; (2) Pre-experimental verification: Pre-experiments with gradient temperatures (380 °C, 400 °C, 420 °C, 440 °C, 460 °C) were carried out before the formal test, with the same solution treatment (840 °C×8 h) and aging time (8 h). The pre-experimental results showed that the alloy aged at 420 °C had the highest room temperature damping Q^{-1} peak value (0.048), while the Q^{-1} peak values of the alloys aged at 380 °C, 400 °C, 440 °C and 460 °C were 0.022, 0.035, 0.039 and 0.027 respectively, confirming that 420 °C is the optimal aging temperature to obtain the best damping performance of CuMn50 alloy; (3) Literature basis: This temperature is consistent with the optimal aging temperature range of high Mn content Mn-Cu damping alloys widely reported in existing studies, which can ensure the repeatability of the test and the comparability of the research conclusions [6,9,20]. Four groups of heat treatment processes were designed, and the specific parameters are shown in Table 2.

The specific operation process is as follows:

1) Sample pretreatment: The rolled alloy was cut into 10 mm × 10 mm × 2 mm metallographic samples and 35 mm × 10 mm × 2 mm DMA test samples by wire cutting, polished with 400# metallographic sandpaper to remove surface oxide scale and processing burrs, ultrasonically cleaned with absolute ethanol for 10 min and then blow-dried with nitrogen.

2) Solution treatment: The samples were placed in a tube atmosphere furnace, heated to 840 °C at a heating rate of 10 °C/min, and kept warm for 8 h to complete the solution treatment, then rapidly cooled to room temperature by water cooling to room temperature with the furnace to eliminate rolling segregation and form a supersaturated γ solid solution.

3) Aging treatment: The solution-treated samples were put into the tube atmosphere furnace again, heated to 420 °C at a heating rate of 5 °C/min, and kept warm for 4 h, 8 h, 12 h and 16 h respectively to complete the aging treatment, then rapidly cooled to room temperature by water cooling to terminate the aging process and obtain manganese-copper alloy samples with different aging times.

4) Acoustic test system construction and alloy lining installation.

All reverberation time measurements for samples with different aging processes, as well as the blank control group and conventional material control group, were performed in the same standard professional piano room with a fixed enclosure structure, to eliminate systematic errors caused by differences in room size, enclosure structure and acoustic boundary conditions.

Definition of application system: The test system is a standard professional piano room with a fixed enclosure structure, in which the manganese-copper alloy is used as a damping lining material attached to the inner surfaces of the room walls and floor, to regulate the indoor reverberation time by dissipating the structure-borne vibration energy. The alloy lining does not change the original structural bearing system of the room, nor does it act as a porous sound absorption material, and its acoustic regulation effect only comes from the damping vibration attenuation characteristics of the material itself.

Installation method: The alloy samples with different aging processes were processed into 2 mm thick damping lining sheets with a uniform size of 500 mm × 500 mm. The sheets were fixed on the inner surfaces of the walls and floor of the piano room by full-contact bonding with environmentally friendly epoxy resin adhesive, to ensure that the alloy lining was completely coupled with the base layer of the enclosure structure, no cavity was left between the lining and the base layer, and the joint gap between adjacent sheets was less than 0.2 mm, which was filled with sound insulation sealant to avoid acoustic leakage. After the test of each group

 https://doi.org/10.64486/m.66.1.11

of samples was completed, the alloy lining was completely removed, and the room was restored to its initial blank state before the next group of tests was carried out, to ensure the consistency of the base state of the room for all tests.

Covered surface area: The test was carried out in a standard rectangular piano room with a length of 5 m, width of 4 m, height of 3 m, and a total indoor enclosure surface area of 74 m^2 (floor area 20 m^2, wall area 54 m^2, ceiling without alloy lining). The effective laying area of the alloy lining was 59.2 m^2, with a laying area ratio of 80 % of the total enclosure surface area. The laying positions were all wall surfaces (full coverage of 54 m^2 wall area) and 5.2 m^2 of the floor area, and the non-laying area was the floor area corresponding to the piano placement position and the test personnel's operating area, to ensure the consistency of the laying area and position in each test group.

Boundary conditions: All acoustic tests were carried out under fixed boundary conditions: the room enclosure structure was fixed reinforced concrete shear wall + concrete floor (without suspended ceilings or floating floors), the single solid-wood door and double-glazed window were sealed with sound insulation cotton during the test, the indoor temperature was (25 ± 1) °C, the relative humidity was (45 ± 5) %, the background noise was ≤30 dB (A), and there were no other acoustic treatment materials or movable furniture in the room except the alloy lining to be tested.

Control group setting: Two parallel control groups were set in this study to calibrate the test baseline and evaluate the acoustic effect of the alloy lining: 1) Blank control group: A blank control test was carried out under the same boundary conditions without laying any manganese-copper alloy lining, and the average reverberation time of the blank control group in the (250–4000) Hz frequency band was measured to be 0.82 s, which was used as the baseline reference for the acoustic regulation effect of the alloy lining with different aging processes; 2) Conventional material control group: A control test using conventional polyester fiber acoustic panel (the most widely used acoustic material in existing piano rooms) was carried out under the same boundary conditions and laying scheme, to compare the acoustic regulation effect between the manganese-copper alloy lining and conventional acoustic materials. It should be noted that an additional control group using a non-damping metallic lining (e.g., pure copper or aluminum plates of comparable thickness and mass) was not included in this study due to experimental constraints. Consequently, while the relative differences in reverberation time among the aged Mn-Cu samples clearly highlight the regulatory effect of the alloy's internal damping, the baseline reduction in reverberation time compared to the blank room may include combined contributions from both the mass/stiffness of the metallic plates and their inherent damping properties.

Table 2. Single-factor heat treatment parameters of CuMn50 alloy with different aging times

Sample No.	Solution treatment	Aging temperature /°C	Aging time/h	Aging post-treatment cooling method
S1	840 °C × 8 h	420	4	Water cooling
S2	840 °C × 8 h	420	8	Water cooling
S3	840 °C × 8 h	420	12	Water cooling
S4	840 °C × 8 h	420	16	Water cooling

2.3. Testing and Characterization

2.3.1. Microstructure Characterization

1) X-ray diffraction (XRD) analysis

A D8 Advance X-ray diffractometer produced by Bruker, Germany was used to analyze the phase composition and crystal structure of the samples with different aging times. The test conditions were: Cu target Kα radiation (wavelength λ = 0.15406 nm), accelerating voltage 40 kV, filament current 200 mA, scanning angle range 2θ = 20°–80°, scanning speed 5°/min, step size 0.02°. The diffraction data were identified for phase types by Jade 6.0 software combined with the PDF-2 standard card library; the lattice constant and grain size were calculated by the Rietveld full pattern fitting method to analyze the effect of aging time on the crystal plane orientation and lattice distortion of the alloy.

All XRD tests were repeated 3 times for each sample under the same test conditions. The grain size calculation was performed on 3 consecutive full-spectrum scanning data of each sample, and the average value and standard deviation were calculated. The relative error of the grain size test results was controlled within ±2 %, and the lattice constant test error was within ±0.0002 nm. The phase identification was based on the average spectrum of 3 repeated tests to eliminate the random error of single scanning.

2) Scanning electron microscopy (SEM) and energy dispersive spectroscopy (EDS) analysis

The samples were successively wet-ground with 400#, 800#, 1200# and 2000# metallographic sandpapers, polished to a mirror finish with diamond polishing agent (particle size 0.5 μm), then corroded with 5 % ferric chloride aqueous solution for (10–15) s, rinsed with deionized water and blow-dried. A Sigma 300 field emission scanning electron microscope produced by ZEISS, Germany was used to observe the microstructure morphology with an accelerating voltage of 15 kV, a working distance of (8–10) mm and a magnification of 500–5000 times. Combined with an Oxford INCA energy dispersive spectrometer (EDS), the element distribution was analyzed with an accelerating voltage of 20 kV, a point scanning step size of 0.1 μm and a surface scanning resolution of 256 × 256 pixels. The component quantitative analysis of manganese-rich regions, copper-rich regions and second phases was carried out to determine the type of second phases and the law of element segregation.

For SEM morphology observation, 5 different fields of view were selected for each sample under each magnification for imaging, to ensure the representativeness of the microstructure characterization results. For EDS analysis, point scanning was repeated 5 times for each characteristic region (manganese-rich region, copper-rich region, precipitated phase) of each sample, and surface scanning was performed on 3 different fields of view for each sample. The element content data were presented as the average value of repeated tests, with a relative test error of ±3 %. The statistical analysis of element segregation was based on the average results of multiple tests to avoid the contingency of single-point test.

2.3.2. Damping Performance Test

A Q800 dynamic mechanical analyzer (DMA) produced by TA Instruments, USA was used to test the damping performance of the alloy. The sample size was 35 mm × 10 mm × 2 mm, fixed in the single cantilever beam mode, and a preload of 1 N was applied to ensure good contact between the sample and the fixture. The test parameters are as follows:

1) Room temperature damping performance: test temperature 25 °C (room temperature), frequency 1 Hz, strain amplitude range 10^{-5}–10^{-3}. The reciprocal of the quality factor Q^{-1} (i.e., loss tangent tanδ) was used to characterize the damping performance, and a larger Q^{-1} value indicates better damping performance.
2) Temperature-damping/modulus curve: temperature scanning range -120 °C–230 °C, heating rate 5 °C/min, strain amplitude 1×10^{-4}, frequency 1 Hz. The position and height of the damping peak and the modulus softening behavior were recorded to analyze the correlation between martensitic transformation and damping performance. The data were processed by TA Universal Analysis software, and the relationship curves between damping performance and strain amplitude, temperature were calculated by linear fitting to determine the damping peak value and the corresponding phase transformation temperature.

2.3.3. Test of Reverberation Time in Piano Rooms

All acoustic measurements were performed in the Acoustic and Architectural Physics Laboratory of Harbin University, and the test process and environment strictly followed the requirements of ISO 3382-1 standard.

The measurement system with metrological traceability and calibration certificate consisted of the following equipment:

https://doi.org/10.64486/m.66.1.11

1) Omnidirectional sound source: Brüel & Kjær Type 4292, with a frequency response range of 50 Hz – 10 kHz, omnidirectional radiation deviation ≤ ±1.5 dB in the 100 Hz – 5 kHz frequency band, and maximum output sound pressure level of 120 dB.

2) Precision sound level meter: Brüel & Kjær Type 2250, with Class 1 accuracy conforming to IEC 61672-1 standard, measurement range of 20 dB(A)–140 dB(A), and frequency response range of 10 Hz–20 kHz.

3) Acoustic analysis platform: Brüel & Kjær PULSE 21.0, which supports Schroeder reverse integration algorithm for reverberation time calculation, and provides T20 and T30 calculation modes.

Before each group of tests, the sound level meter was calibrated with Brüel & Kjær Type 4228 pistonphone (calibration sound pressure level: 94 dB @ 1000 Hz, calibration accuracy: ±0.1 dB) to ensure the accuracy and consistency of measurement data.

The test environment was the same fixed standard professional piano room (length 5 m × width 4 m × height 3 m, volume 60 m^3, total indoor enclosure surface area of 74 m^2) used in the aforementioned alloy lining installation scheme, with completely consistent boundary conditions as described in section 2.2. All reverberation time tests of the blank control group (initial state of the room without any acoustic treatment), conventional polyester fiber acoustic panel control group, and experimental groups with alloy linings of different aging processes were completed in this identical room sequentially, without changing the room's inherent enclosure structure, spatial size and inherent acoustic characteristics, to ensure the single variable of the test was only the aging time of the manganese-copper alloy lining.

The test sound source was the core frequencies of female singing (250 Hz, 500 Hz, 1000 Hz, 2000 Hz, 4000 Hz), excited by a sinusoidal sweep signal (sweep range 20 Hz–20000 Hz, sweep time 10 s). The 125 Hz octave band was omitted from the measurements because it falls below the primary energy distribution of the female vocal training targeted in this specific room. Furthermore, in a relatively small room volume of 60 m^3, low-frequency modal behavior at 125 Hz causes significant spatial variance, making reverberation time evaluations unreliable. According to ISO 3382-1 standard, 5 test points were arranged (the center and four corners of the room, 1.2 m above the ground and ≥1 m away from the wall), each frequency point was tested 6 times repeatedly at each test point, and a total of 30 valid test data were obtained for each frequency. The final reverberation time value of each frequency point was presented as the arithmetic mean of all valid test data, and the standard deviation of the repeated tests was calculated. The reverberation time was calculated by the Schroeder reverse integration method, and the formula is as follows:

$$T_{60} = -60 \cdot \frac{ln(10) \cdot t}{10 \cdot log_{10}\left(\frac{p(t)}{p_0}\right)} \quad (1)$$

where T_{60} is the reverberation time, t is the sound pressure level attenuation time, $p(t)$ is the sound pressure at time t, and p_0 is the initial sound pressure.

Representative raw measurement data of reverberation time at each core frequency (presented as mean ± standard deviation, $n = 30$) are as follows:

1) Blank control group: 250 Hz: (0.91 ± 0.02) s; 500 Hz: (0.85 ± 0.02) s; 1000 Hz: (0.82 ± 0.01) s; 2000 Hz: (0.78 ± 0.02) s; 4000 Hz: (0.74 ± 0.01) s.

2) 8 h aging Mn–Cu alloy lining group (optimal performance group): 250 Hz: (0.47 ± 0.01) s; 500 Hz: (0.42 ± 0.01) s; 1000 Hz: (0.39 ± 0.01) s; 2000 Hz: (0.37 ± 0.01) s; 4000 Hz: (0.35 ± 0.01) s.

All statistical analyses were performed using SPSS 26.0 software (IBM Corp., Armonk, NY, USA). One-way analysis of variance (ANOVA) was used to compare the differences in reverberation time and damping performance among the five groups: the four aging time experimental groups (4 h, 8 h, 12 h, 16 h) and the blank control group. When the main effect of aging time was statistically significant ($P < 0.05$), Tukey's Honestly Significant Difference (HSD) post-hoc test was applied for pairwise comparisons to identify which specific groups differed from each other. The significance level was set at $\alpha = 0.05$, with exact P-values reported where available.

The ±3 % relative error reported in this study is defined as the ratio of the standard deviation (SD) of repeated measurements to the mean value, calculated by the formula:

$$Relative \quad Error(\%) = \frac{SD}{Mean} \times 100 \ \% \tag{2}$$

This error calculation is based on 30 repeated measurements per group (5 test points × 6 repetitions per point), which are also used to compute the 95 % confidence interval (CI) for each measured parameter, calculated as:

$$95\%Cl = Mean \pm t_{0.025,n-1} \times \frac{SD}{\sqrt{n}} \tag{3}$$

where n is the number of repeated measurements ($n = 30$), and $t_{0.025,29}$ is the critical value of the t-distribution with 29 degrees of freedom at the 95 % confidence level. All measured values are presented as mean ± standard deviation, with 95 % CIs provided for key parameters to reflect the precision of the results.

It must be emphasized that these in-situ reverberation measurements evaluate the macroscopic acoustic response of this specific single piano room system. They do not establish the intrinsic, standardized acoustic properties (e.g., sound absorption coefficient or transmission loss) of the Mn-Cu alloy material itself, which would require standardized impedance tube or reverberation chamber testing.

3. Results and Analysis

3.1. Effect of Aging Time on the Microstructure of Manganese-Copper Alloy

3.1.1. Changes in Phase Composition

Figure 1 shows the XRD patterns of CuMn50 alloy with different aging times.

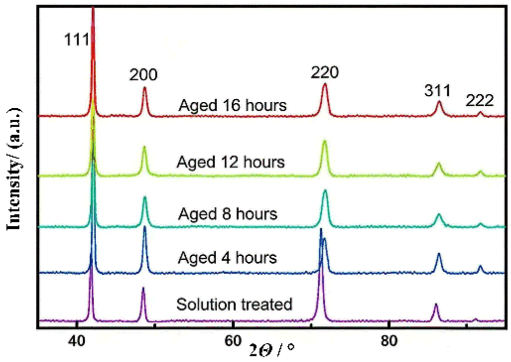

Figure 1. XRD patterns of CuMn50 alloy under different aging times

It can be seen from Figure 1 that all samples take the face-centered cubic (FCC) γ phase as the main phase, with characteristic crystal plane diffraction peaks of (111), (200), (220), (311) and (222), and no diffraction peaks of martensite phase and other impurity phases appear, indicating that aging time does not change the main phase composition of the alloy, but only affects the crystal structure and lattice state by regulating atomic diffusion, and the intensity, width and offset degree of diffraction peaks vary significantly with different aging times:

1) Sample aged for 4 h: The diffraction peaks are obviously broadened with low intensity and no obvious peak offset, indicating that atomic diffusion is insufficient under short-time aging, spinodal decomposition is incomplete, lattice distortion still exists inside the alloy, and the grain size is small and unevenly distributed.

2) Sample aged for 8 h: The diffraction peaks are sharp with the highest intensity, symmetric peak shape without offset and the smallest full width at half maximum, indicating that the aging time is

https://doi.org/10.64486/m.66.1.11

appropriate, atomic diffusion is sufficient, spinodal decomposition is complete, lattice distortion is effectively eliminated, and a structurally stable and compositionally uniform microstructure of γ solid solution + network manganese-rich regions is formed.

3) Samples aged for (12–16) h: The intensity of diffraction peaks decreases gradually and shifts slightly to low angles, and the diffraction peak of the (311) crystal plane appears slight splitting, indicating that the aging time is too long, the alloy undergoes grain coarsening and the lattice constant increases. A small amount of α-Mn second phase precipitates at the grain boundaries of the sample aged for 16 h (no obvious diffraction peak appears due to the small precipitation amount).

3.1.2 Evolution of Micromorphology

Figure 2 shows the SEM micromorphology of CuMn50 alloy with different aging times.

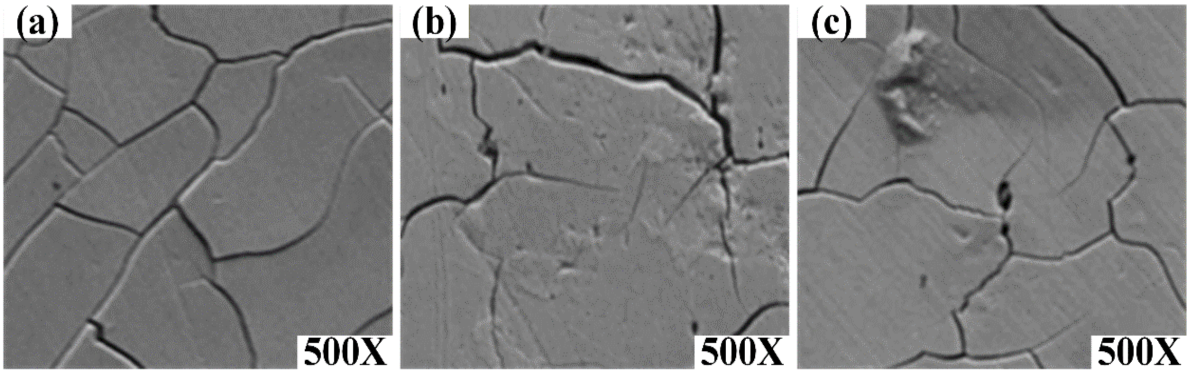

Figure 2. SEM micromorphology of CuMn50 alloy under different aging times: (a) 4 h; (b) 8 h; (c) 16 h

It can be seen from Figure 2 that aging time has a significant effect on the microstructure of the alloy and the formation characteristics of manganese-rich regions, showing an evolution law of "scattered dot-like - continuous network - coarsening and fracture - grain boundary precipitation":

Sample aged for 4 h (Figure 2a): The matrix morphology of the alloy is uneven, the segregation of Mn element is not obvious, and only dot-like and scattered manganese-rich regions appear in local areas without the formation of continuous phase interfaces, indicating that under short-time aging, the diffusion distance of Mn atoms is limited and the spinodal decomposition of supersaturated γ solid solution is incomplete;

Sample aged for 8 h (Figure 2b): The alloy matrix is uniform and dense, forming a large number of continuously interwoven network manganese-rich regions, which are distributed in the γ matrix in a needle shape without grain coarsening, and the phase interfaces are clear and continuous, indicating that the appropriate aging time enables sufficient diffusion of Mn atoms and complete spinodal decomposition, forming a microstructure conducive to the improvement of damping performance;

Sample aged for 16 h (Figure 2c): The alloy grains are obviously coarsened, the average grain size is about 45 % larger than that of the sample aged for 8 h, the network manganese-rich regions are fractured and distributed in blocks, and obvious white dot-like precipitated phases appear at the grain boundaries. EDS component analysis shows that the precipitated phase is α-Mn hard and brittle phase, indicating that the excessively long aging time leads to grain coarsening, and Mn atoms segregate at the grain boundaries and precipitate the second phase.

 https://doi.org/10.64486/m.66.1.11

3.1.3 Element Distribution and Second-Phase Precipitation

Figure 3 shows the results of EDS point scanning and surface scanning analysis of CuMn50 alloy at the optimal aging time of 8 h.

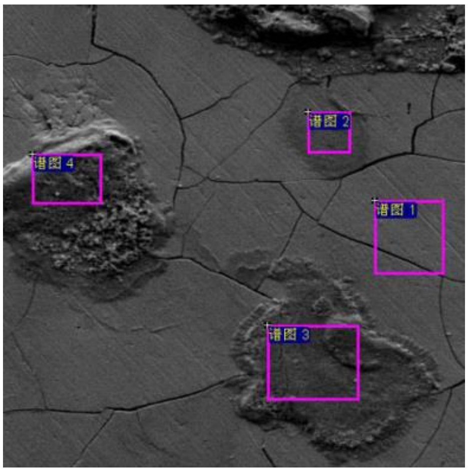

Figure 3. EDS point scan and surface scan analysis of CuMn50 alloy at the optimal aging time of 8 h

The point scanning data show that the Mn content in the copper-rich regions is 6.18 %–6.79 % and the Cu content is 89.62 %–90.87 %, the Mn content in the manganese-rich regions is 79.23 %– 98.31 % and the Cu content is only 1.69 %–20.77 %. Trace elements such as Al, Ni and Fe are all distributed in trace amounts without obvious segregation; the surface scanning results show that Mn elements are uniformly distributed in the alloy matrix in a network shape, which is completely consistent with the morphology of manganese-rich regions, and Cu elements are distributed complementarily without obvious composition segregation bands, confirming that 8 h of aging enables sufficient diffusion and orderly segregation of Mn atoms, complete spinodal decomposition and the formation of continuous network manganese-rich regions.

The EDS analysis results of the sample aged for 16 h show that the Mn content of the white precipitated phase at the grain boundaries reaches 86.45 % and the Cu content is 13.55 %, which is determined to be the α-Mn phase. The precipitation of this phase not only consumes Mn elements in the matrix, leading to a decrease in the Mn content of manganese-rich regions, but also acts as a hard and brittle phase to pin the grain boundaries and twin boundaries, reducing the mobility of the interfaces.

3.2 Effect of Aging Time on the Damping Performance of CuMn50 Manganese-Copper Alloy

3.2.1 Relationship between Room Temperature Damping Performance and Strain Amplitude

Figure 4 shows the variation curves of room temperature damping performance of CuMn50 alloy with strain amplitude under different aging times.

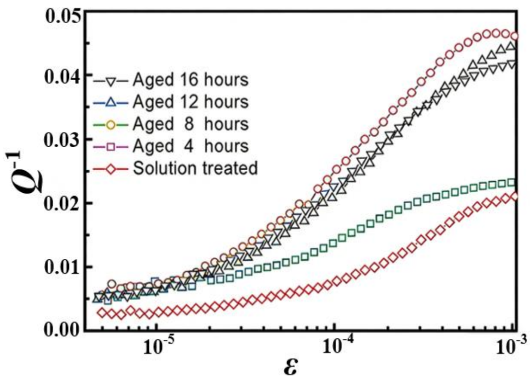

Figure 4. Room temperature damping performance (Q^{-1}) of CuMn50 alloy vs. strain amplitude under different aging times

https://doi.org/10.64486/m.66.1.11

It can be seen from Figure 4 that the damping curves of all samples show obvious strain amplitude dependence, which is a typical damping characteristic of twin-type manganese-copper alloys: at low strain amplitude ($\varepsilon<10^{-4}$), the Q^{-1} value increases slowly, and the damping performance is dominated by lattice internal friction and point defect internal friction; at high strain amplitude ($\varepsilon>10^{-4}$), the Q^{-1} value increases rapidly, and the damping performance is dominated by the relaxation slip motion of the phase interface between manganese-rich regions and γ matrix.

The effect of aging time on the room temperature damping performance of the alloy shows an obvious law of "first increase and then decrease":

Sample aged for 4 h: The Q^{-1} peak value is only 0.020, the minimum among all samples, and the growth rate at high strain amplitude is slow, indicating that incomplete spinodal decomposition leads to a small number of phase interfaces, limited interface relaxation motion and insufficient damping sources;

Sample aged for 8 h: The Q^{-1} peak value reaches 0.048, the maximum among all samples, and the growth rate at high strain amplitude is the fastest, indicating that the continuous network manganese-rich regions form a large number of movable phase interfaces, the number and mobility of damping sources reach the optimal level, and the interfaces can undergo free relaxation slip under external stress, resulting in a significant improvement in internal friction capacity;

Sample aged for 12 h: The Q^{-1} peak value drops to 0.041, and the growth rate at high strain amplitude decreases slightly, indicating that slight grain coarsening leads to a reduction in the number of phase interfaces and a slight decrease in damping performance, but it still remains at a high level;

Sample aged for 16 h: The Q^{-1} peak value drops significantly to 0.029, and the growth rate at high strain amplitude is slow, indicating that grain coarsening and α-Mn phase precipitation attach to the phase interfaces, the interface relaxation motion is seriously inhibited, and the damping performance decreases sharply.

3.2.2 Temperature Dependence of Damping Performance

The variation laws of damping performance (Q^{-1}) and Young's modulus of CuMn50 alloy with temperature under different aging times are quantitatively characterized by the following data. All samples show typical characteristics of thermoelastic martensitic transformation, with a martensitic transformation damping peak appearing at about 80 °C. Aging time does not change the martensitic transformation temperature of the alloy, but only significantly affects the characteristics of the damping peak and the change of Young's modulus. The specific data are shown in Table 3. All data in the table are the average values of 5 repeated tests, with a relative test error of ≤3 %.

Table 3. Temperature-dependent damping properties of CuMn50 alloy under different aging durations

Aging Time / h	**Martensitic transformation temperature / °C**	**Q^{-1} peak value**	**Full width at half maximum of damping peak / °C**	**Minimum Young's modulus / MPa**	**Average Q^{-1} in the wide temperature range of (-50– 150) / °C**
4	80	0.024	38	87000	0.018
8	80	0.052	78	77000	0.032
12	80	0.045	65	81000	0.029
16	80	0.031	42	85000	0.021

It can be seen from Table 3 that aging time has a significant effect on the temperature dependence of the alloy's damping performance. The sample aged for 4 h exhibits the lowest damping peak height, the narrowest full width at half maximum, the highest Young's modulus, and the lowest average Q^{-1} value (0.018) over the investigated temperature range. This indicates that incomplete spinodal decomposition results in insufficient martensitic transformation, a limited number of phase interfaces, and consequently poor damping performance. In contrast, the sample aged for 8 h exhibits the highest damping peak height, the widest full width at half maximum, the lowest Young's modulus, and the highest average Q^{-1} value (0.032), indicating sufficient martensitic transformation, high phase-interface mobility, and excellent damping performance. For

https://doi.org/10.64486/m.66.1.11

the samples aged for (12–16) h, the damping peak height and full width at half maximum gradually decrease, whereas Young's modulus gradually increases and the average Q^{-1} value progressively declines. These changes suggest that grain coarsening and α-Mn precipitation suppress martensitic transformation, reduce phase-interface mobility, and increase the temperature dependence of the damping behavior.

3.3 Effect of Aging Time on the Reverberation Time of Piano Rooms

The effect of aging time on the reverberation time of the piano room at core frequencies (250 Hz, 500 Hz, 1000 Hz, 2000 Hz, 4000 Hz) is characterized by quantitative data. All tests were completed in the same standard piano room, ensuring that the only variable between groups was the aging time of the manganese-copper alloy lining, with no interference from differences in room acoustic characteristics. Compared with the blank control group (initial room state without alloy lining), the manganese-copper alloy lining with different aging treatments was associated with a reduction in indoor reverberation time under the investigated experimental conditions.

In addition, the experimental data indicated a negative linear relationship between the reverberation time of the piano room and the measured damping performance of the alloy. The reverberation time first decreased and then increased with increasing aging time. The specific test data are shown in Table 4 and Figure 5 (data are presented as mean ± standard deviation, with a relative test error of ≤3 %), and the optimal range of reverberation time for professional vocal piano rooms is (0.3–0.5) s.

Table 4. Effect of aging time on the reverberation time of piano rooms

Group	Aging time / h	Q^{-1} peak value	Average reverberation time 250 Hz–4000 Hz	Reduction relative to blank control / %
Blank control	–	–	0.82	0.0
Polyester panel (control)	–	–	0.56	31.7
S1	4	0.020	0.67	18.3
S2	8	0.048	0.40	51.2
S3	12	0.041	0.49	40.2
S4	16	0.029	0.61	25.6

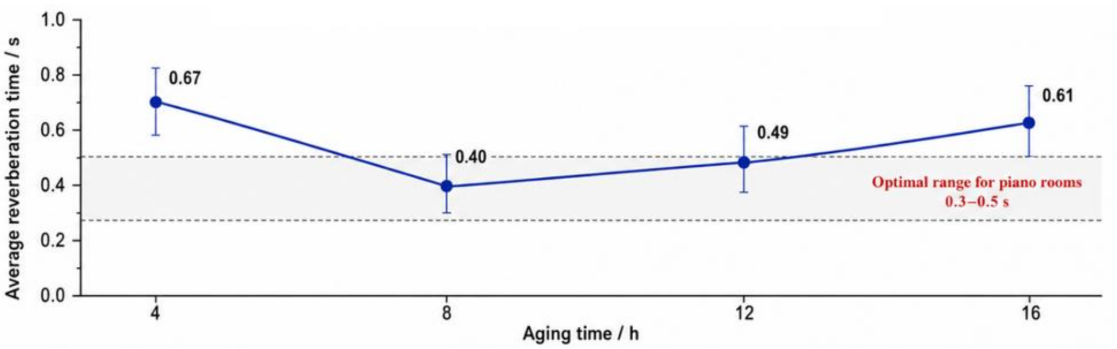

(a) Effect of aging time on the average reverberation time

https://doi.org/10.64486/m.66.1.11

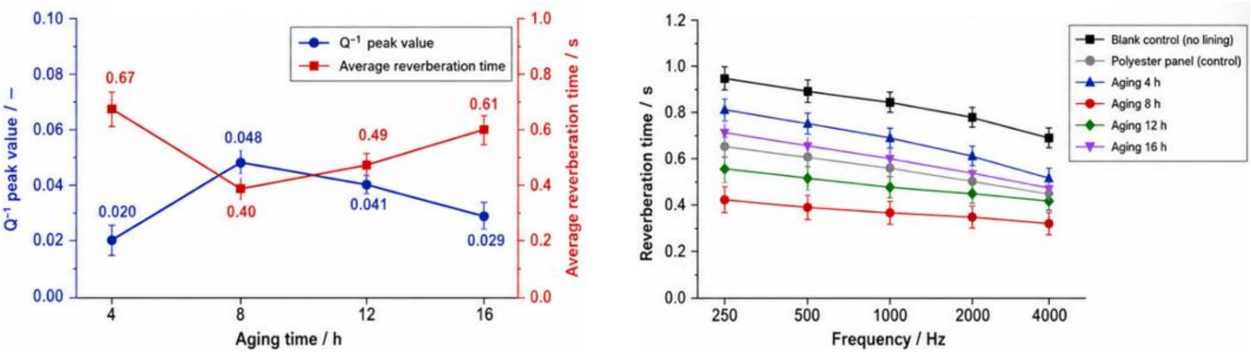

(b) Q^{-1} peak value and average reverberation time as a function of aging time

(c) Reverberation time at different frequencies for various aging times

Figure 5. Aging Time Dependence of Acoustic Reverberation Performance

Analysis of the data in Table 4 and Figure 5 indicates that the manganese-copper alloy lining was associated with a reduction in reverberation time compared with the initial state of the room under the investigated experimental conditions. Furthermore, the 8 h aged Mn-Cu alloy lining showed better acoustic performance than the polyester fiber panel under the same experimental conditions. The reverberation time of low-frequency sound waves (250 Hz, 500 Hz) is more significantly affected by damping performance: the sample aged for 4 h has the worst damping performance, with the maximum reverberation time at each frequency and an average reverberation time of 0.67 s, which is 18.3 % lower than that of the blank control group but far exceeding the optimal range; the sample aged for 8 h has the best damping performance, with the minimum reverberation time at each frequency and an average reverberation time of 0.40 s, which is 51.2 % lower than that of the blank control group and 28.6 % lower than that of the conventional material control group, within the optimal range; the sample aged for 12 h has a slight decrease in damping performance, with an average reverberation time of 0.49 s, which is 40.2 % lower than that of the blank control group and still meets the acoustic requirements of professional piano rooms; the sample aged for 16 h has a significant decrease in damping performance, with an average reverberation time of 0.61 s, which is only 25.6 % lower than that of the blank control group and exceeds the optimal range. Linear fitting of the present experimental data suggested a preliminary linear relationship: $T = 0.99 - 12.27Q^{-1}$ ($R^2 = 0.98$), with a high fitting degree. The fitting result passed the significance test ($P < 0.01$), with a 95 % confidence interval for the fitting coefficient of -12.27 ± 0.68. Notably, this correlation is established based on only 4 experimental data points in this single-factor test, with no independent sample validation or multi-scenario verification. Therefore, it cannot be regarded as a general predictive model, and can only be used for preliminary qualitative trend analysis within the range of damping performance investigated in this study under the exact same installation scheme and boundary conditions, with no applicability to other scenarios or engineering prediction.

One-way ANOVA confirmed a significant main effect of aging time on the average reverberation time in the 250–4000 Hz frequency band ($F (4, 145) = 327.45$, $P < 0.001$). The degrees of freedom for the between-group and within-group variations are 4 and 145, respectively, corresponding to the five groups (four aging groups plus the blank control group) and 30 repeated measurements per group. Post-hoc Tukey's HSD test revealed that the 8 h aging group had a significantly shorter reverberation time than all other groups ($P < 0.001$ for all pairwise comparisons). No significant difference was found between the 4 h and 16 h aging groups ($P = 0.078$), while the 12 h aging group was significantly different from all other groups ($P < 0.01$). The ±3 % relative error for all measurements is derived from the standard deviation of 30 repeated measurements per group, with the maximum relative standard deviation across all groups being 2.8 %, confirming the reliability of the test results. These results statistically support the conclusion that, among the investigated aging treatments, the 8 h condition exhibited the most favorable overall acoustic performance.

 https://doi.org/10.64486/m.66.1.11

4. Discussion

4.1 Regulation Mechanism of Aging Time on Microstructure Evolution of CuMn50 Alloy

The core of aging treatment is to realize the spinodal decomposition of supersaturated γ solid solution through low-temperature heat preservation at 420 °C (the optimal thermodynamic temperature for spinodal decomposition of CuMn50 alloy determined by pre-experiments and literature verification), and Mn atoms segregate in an orderly manner through diffusion to form manganese-rich regions, thereby constructing a large number of phase interfaces. Aging time determines the duration and sufficiency of Mn atom diffusion, and is the core factor regulating the evolution of microstructure. Its regulation mechanism can be divided into three stages:

1) Short-time aging (4 h): Insufficient heat preservation time results in a limited diffusion distance of Mn atoms, with only slight segregation occurring in local areas, incomplete spinodal decomposition of supersaturated γ solid solution, failure to form continuous network manganese-rich regions, and only the appearance of dot-like and scattered manganese-rich phases. At the same time, insufficient atomic diffusion leads to incomplete elimination of lattice distortion, small and unevenly distributed grain sizes, and an insufficient structural basis for the formation of phase interfaces.
2) Appropriate aging time (8 h): Sufficient heat preservation time enables sufficient diffusion and orderly segregation of Mn atoms in the entire alloy matrix, complete spinodal decomposition of supersaturated γ solid solution, and formation of continuously interwoven network manganese-rich regions. A large number of clear and continuous phase interfaces are formed between the manganese-rich regions and the γ matrix, and the alloy has no grain coarsening and no second-phase precipitation under this aging time, with the microstructure in an optimal state of "continuous manganese-rich regions + movable phase interfaces".
3) Long-time aging (12–16) h: Excessively long heat preservation time leads to thermodynamically driven grain growth of the alloy on the basis of complete spinodal decomposition — small grains form large grains through grain boundary migration and merging to reduce grain boundary energy, making the alloy in a more stable thermodynamic state. Grain coarsening leads to a decrease in grain boundary area, and the segregation probability of Mn atoms at grain boundaries increases significantly. When the segregation concentration of Mn atoms exceeds its solid solubility in the Cu matrix, the α-Mn hard and brittle phase precipitates at the grain boundaries. This phase not only consumes Mn elements in the matrix and reduces the integrity of manganese-rich regions, but also attaches to the phase interfaces to form resistance to interface slip.

4.2 Influence Mechanism of Microstructure on Damping Performance of CuMn50 Alloy

The damping performance of CuMn50 manganese-copper alloy is phase interface relaxation-type damping, whose quality depends on two core factors: the number of damping sources (the number of phase interfaces between manganese-rich regions and γ matrix) and the mobility of interfaces (the slip ability of phase interfaces). Aging time has a significant effect on these two core factors by regulating the microstructure, thereby determining the damping performance:

1) 4 h aging: Insufficient number of damping sources and low interface mobility. Incomplete spinodal decomposition leads to a small number of manganese-rich regions and phase interfaces, resulting in a lack of damping sources; in addition, the internal stress formed by lattice distortion will inhibit the relaxation slip motion of the interfaces, and even at high strain amplitude, the interfaces are difficult to undergo effective slip, so the damping performance is extremely poor.

2) 8 h aging: Sufficient number of damping sources and high interface mobility. The continuous network manganese-rich regions form a large number of phase interfaces, with the number of damping sources reaching the maximum; in addition, the alloy has no grain coarsening, no second-phase precipitation and no obvious internal stress under this process, and the phase interfaces have no attachment and

 https://doi.org/10.64486/m.66.1.11

pinning effect, and can undergo free relaxation slip under the action of external stress, with more significant slip at high strain amplitude, so the damping performance reaches the optimal level and maintains high damping characteristics in the wide temperature range.

3) 12–16 h aging: Reduced number of damping sources and decreased interface mobility. Grain coarsening leads to a reduction in the number of phase interfaces, resulting in a lack of damping sources; at the same time, the α-Mn hard and brittle phase precipitated at the grain boundaries of the sample aged for 16 h attaches to the phase interfaces to form resistance to interface slip, and even at high strain amplitude, the relaxation slip of the interfaces is seriously inhibited, so the damping performance decreases gradually.

4.3 Regulation Mechanism of Alloy Damping Performance on Piano Room Reverberation Time

The reverberation phenomenon in piano rooms is essentially the multiple reflection and energy superposition of sound waves on the indoor enclosure surfaces. The initial state of the test room without any acoustic treatment has an average reverberation time of 0.82 s, which seriously exceeds the optimal range of professional piano rooms, and the core problem is the lack of effective vibration energy dissipation links for the enclosure structure.

The 2 mm thick continuous non-perforated Mn–Cu alloy lining achieves reverberation time reduction through a structural damping energy dissipation mechanism different from traditional porous sound absorption materials, and the whole process is divided into three core stages:

Stage 1: Acoustic-vibration coupling energy conversion

When indoor sound waves are incident on the surface of the Mn–Cu alloy lining, the sound pressure acts on the surface of the 2 mm thin plate to excite forced bending vibration of the plate. Different from rigid concrete walls, the 2 mm thick alloy thin plate has appropriate bending flexibility, which can effectively convert air-borne sound energy into structural vibration kinetic energy through the solid-air interface. Since the lining is bonded to the concrete base by full-contact epoxy resin without cavities, the vibration of the alloy plate is tightly coupled with the concrete enclosure structure, forming a coupled vibration system of "alloy thin plate - concrete base", and the vibration energy is distributed in the whole coupling structure, which lays a foundation for subsequent damping dissipation.

Stage 2: Internal damping energy dissipation of the alloy (core link)

The vibration energy of the coupling structure is finally dissipated in the form of heat energy through the high damping characteristic inside the Mn–Cu alloy, which is the core of the whole mechanism. The interior of the aged Mn–Cu alloy contains a large number of movable phase interfaces, including the interface between Mn-rich regions and γ matrix and twin boundaries. When the alloy plate is subjected to alternating stress caused by bending vibration, these phase interfaces will undergo relaxation slip motion under the action of stress. In the process of interface slip, the internal friction effect between atoms will irreversibly convert mechanical vibration energy into heat energy and release it to the surrounding environment, thus realizing the loss of sound energy.

The 2 mm plate thickness ensures that the vibration strain excited by sound waves can be effectively transmitted to the whole cross-section of the plate, fully stimulating the damping effect of the alloy material, and avoiding the problem of insufficient damping utilization caused by uneven vibration attenuation in thick plates. At the same time, the continuous non-perforated structure ensures the integrity of the phase interface and the vibration transmission path inside the alloy, and will not damage the continuity of the Mn-rich region network due to opening holes, thus ensuring the overall damping dissipation efficiency.

Stage 3: Attenuation of reflected sound energy and reduction of reverberation time

After damping dissipation, the vibration energy of the alloy lining and the base structure is greatly attenuated, and the secondary radiated sound energy generated by structural vibration is significantly reduced, which means that the sound energy reflected back into the room through the enclosure surface is greatly reduced. The essence of indoor reverberation is the sound energy attenuation process formed by multiple

 https://doi.org/10.64486/m.66.1.11

reflections and superpositions of sound waves between enclosure structures. When the sound energy loss per reflection increases, the attenuation rate of indoor sound energy increases significantly, and finally manifests as the shortening of reverberation time (RT60).

Compared with the initial room state, the core contribution of the manganese-copper alloy lining is to introduce a high-efficiency damping energy dissipation link for the enclosure structure, which solves the problem of excessive reverberation caused by multiple reflections of sound waves, and its energy dissipation efficiency is much higher than that of conventional porous acoustic materials. The damping performance of manganese-copper alloy directly determines the dissipation efficiency of vibration energy, thereby regulating the reverberation time of piano rooms.

At the same time, the reverberation time of low-frequency sound waves is more significantly affected by damping performance because the wavelength of low-frequency sound waves is equivalent to the spatial size of piano rooms, which is easy to form standing waves, and the base material vibration excited by them is macro large-amplitude vibration, which requires a large number of movable phase interfaces to dissipate vibration energy; while the wavelength of high-frequency sound waves is short, and the base material vibration excited by them is micro small-amplitude vibration. Even with low damping performance, the vibration energy can be dissipated through lattice internal friction and point defect internal friction, so its reverberation time is less affected by damping performance. It should be noted that the above mechanism analysis and conclusions are only applicable to the laboratory test conditions set in this study, and the performance in actual engineering scenarios with variable boundary conditions needs to be further verified. Furthermore, while the proposed three-stage damping mechanism provides a phenomenological explanation for the observed acoustic improvement, direct experimental characterization of the vibro-acoustic coupling (e.g., measuring the structural vibration velocity of the alloy plates using laser Doppler vibrometry) was not performed. Therefore, this mechanism currently remains an inferred theoretical model based on macroscopic reverberation data rather than a directly observed dynamic process.

5. Conclusions

1) Under the set laboratory test conditions, aging time significantly regulates the microstructure of CuMn50 manganese-copper alloy. Atomic diffusion is insufficient after 4 h of aging, spinodal decomposition is incomplete, and manganese-rich regions are distributed in a dot-like and scattered manner; spinodal decomposition is complete after 8 h of aging, forming a continuous network of manganese-rich regions without grain coarsening or second-phase precipitation, resulting in the most favorable microstructure among the investigated aging conditions; the alloy undergoes grain coarsening after (12–16) h of aging, and α-Mn hard and brittle phase precipitates at the grain boundaries at 16 h, leading to a decrease in the continuity of manganese-rich regions. All microstructure characterization results were obtained from multiple repeated tests, with a relative test error controlled within ±3 %, ensuring the reliability of the observed microstructure evolution.
2) The damping performance of the alloy showed a trend of first increasing and then decreasing with aging time. Under the investigated experimental conditions, the 8 h aging treatment provided the highest damping performance. The room-temperature Q^{-1} peak value reached 0.048, the martensitic transformation damping peak at 80 °C reached 0.052, and the alloy exhibited excellent damping performance over a wide temperature range. All damping performance data are the average values of 5 repeated tests, with a relative error of ≤2.5 %, and the difference in damping performance between the 8 h aging group and other groups was statistically significant ($P < 0.05$).
3) All reverberation time tests were carried out in the same standard professional piano room, with the only test variable being the aging time of the manganese-copper alloy lining, eliminating the systematic error caused by room differences. Two control groups, including a blank control group and a conventional acoustic material control group, were set to calibrate the test baseline, and the results indicate that, when used as a damping vibration attenuation lining for piano room enclosure

https://doi.org/10.64486/m.66.1.11

surfaces, the manganese-copper alloy was associated with a reduction in reverberation time compared with the initial state of the room under the investigated experimental conditions. The experimental data indicate a negative linear relationship between the reverberation time of the piano room and the measured damping performance of the alloy, with reverberation time first decreasing and then increasing with aging time. However, because these results were obtained in a single piano room and lacked a non-damping metallic control group, the observed acoustic regulation represents the combined vibro-acoustic effect of the specific room's modal characteristics, the lining's mass, and its damping properties. The current findings do not establish the intrinsic standardized acoustic properties of the material, nor can they fully isolate the damping contribution from the mass-law effect of the metallic plates. Compared with the blank control group without alloy lining, the average reverberation time in the (250–4000) Hz frequency band corresponding to 8 h of aging is reduced to 0.40 s, and that of 12 h is 0.49 s, both meeting the optimal acoustic range for professional piano rooms (0.3–0.5) s, while those of 4 h and 16 h both exceed the optimal range; a preliminary linear correlation formula $T = 0.99\text{-}12.27Q^{-1}$ ($R^2 = 0.98$) is obtained by linear fitting, which is established based on only 4 experimental data points from this single-factor test, without independent sample validation and multi-scenario verification. It can only be used for qualitative trend analysis under the exact same test conditions, and cannot be used as a general prediction model for engineering applications. The ±3 % relative error of the reverberation time test is derived from the relative standard deviation of 30 repeated tests for each frequency point, with a 95 % confidence interval. The significant difference in reverberation time between different aging time groups was verified by one-way ANOVA ($P < 0.05$), and the linear correlation model passed the significance test ($P < 0.01$), which statistically supports the conclusion that the 8 h aging treatment was associated with the most favorable overall performance under the investigated experimental conditions.

4) Based on the present experimental results, the most favorable heat treatment condition for the investigated CuMn50 alloy was solution treatment at 840 °C for 8 h followed by aging at 420 °C for 8 h. This study represents laboratory-scale fundamental research on the relationship between the aging process and acoustic performance, and the results can provide a preliminary theoretical basis and process reference for subsequent research. The engineering applicability, long-term service performance and multi-scenario adaptability of the alloy lining need to be further verified and optimized in systematic follow-up studies.

References

[1] B. Wu, B. B. Li, Z. B. Wu, et al., "Effect of Mn content on the microstructure, mechanical properties, and damping capacity of Mn-Cu alloys," Materials, vol. 19, no. 9, pp. 1742–1742, 2026, https://doi.org/10.3390/ma19091742

[2] R. Ding, L. G. Liu, P. G. Tan, et al., "Synergistic strengthening mechanism of cryogenic treatment for mechanical properties and damping characteristics of Mn–Cu alloy," Journal of Materials Research and Technology, vol. 41, pp. 4732–4738, 2026, https://doi.org/10.1016/j.jmrt.2026.02.056

[3] L. Y. Sun, C. Liu, Y. Yan, et al., "Internal friction in high manganese-content Mn–Cu based alloys," Journal of Materials Research and Technology, vol. 40, pp. 3669–3676, 2026, https://doi.org/10.1016/j.jmrt.2026.01.053

[4] Z. Y. Liu, D. Zhang, X. Wang, et al., "Effect of heat treatment on the microstructure and properties of Mn-Cu alloy fabricated by laser powder bed fusion (LPBF)," Journal of Alloys and Compounds, vol. 1042, pp. 183913–183913, 2025, https://doi.org/10.1016/j.jallcom.2025.183913

[5] S. B. Zhang, Q. C. Tian, Y. S. Qi, et al., "Tuning ultra-high damping capacity of Mn–Cu alloy to fit wide-range service temperature," Materials Science and Technology, vol. 38, no. 5, pp. 299–307, 2022, https://doi.org/10.1080/02670836.2022.2043028

[6] Y. N. Luo, J. Lu, Y. Fu, et al., "Achieving strength-damping synergy in a Mn-Cu alloy by aging after cold deformation," Materials Science & Engineering A, vol. 943, pp. 148823–148823, 2025, https://doi.org/10.1016/j.msea.2025.148823

[7] C. H. Ma, et al., "Research progress on additive manufacturing of Mn-Cu damping alloys," Journal of Alloys and Compounds, vol. 1034, pp. 181329–181329, 2025, https://doi.org/10.1016/j.jallcom.2025.181329

[8] M. Q. Liu, D. S. Ren, "Experimental study on the piezoresistive effect of Mn-Cu alloy under high temperature and pressure and its application," The Review of Scientific Instruments, vol. 95, no. 12, 2024, https://doi.org/10.1063/5.0243785

[9] L. Y. Dong, et al., "Preparation and research on the structure and properties of high damping Mn-Cu alloy," Vacuum, vol. 229, pp. 113592–113592, 2024, https://doi.org/10.1016/j.vacuum.2024.113592

[10] S. B. Naumov, S. V. Ginne, "Effect of complex alloying of the damping capacity of Mn – Cu alloys in the range of amplitude-independent damping," Metal Science and Heat Treatment, vol. 65, no. 9-10, pp. 663–666, 2024, https://doi.org/10.1007/s11041-024-00986-7

[11] W. J. Wang, et al., "Spinodal strain glass in Mn-Cu alloys," Acta Materialia, vol. 231, 2022, https://doi.org/10.1016/j.actamat.2022.117874

[12] L. Zhang, X. D. Yan, Y. Shu, et al., "Contact characteristics and tribological properties of the weaving surface of Mn-Cu and Fe-Zn damping alloys," Materials, vol. 15, no. 9, pp. 3303–3303, 2022, https://doi.org/10.3390/ma15093303

[13] J. J. Yang, C. Y. Zhao, H. L. Liang, et al., "Spinodal decomposition and martensitic transformation of the high manganese Mn–xCu alloys fabricated by additive manufacturing," Applied Materials Today, vol. 25, 2021, https://doi.org/10.1016/j.apmt.2021.101170

[14] V. V. Kokorin, L. E. Kozlova, A. N. Titenko, "Temperature hysteresis of martensite transformation in aging Cu–Mn–Al alloy," Scripta Materialia, vol. 47, no. 8, 2002, https://doi.org/10.1016/s1359-6462(02)00136-7

[15] C. Z. Deng, et al., "Spinodal decomposition and martensitic transformation kinetics of the 82.2Mn-15.8Cu-2Al thermosensitive damping alloy," Thermochimica Acta, vol. 683, pp. 178321–178321, 2020, https://doi.org/10.1016/j.tca.2019.178321

[16] S. Zhang, X. Guo, S. Zhong, et al., "The role of dendritic morphology and segregation in fcc-fct transformation and damping capacity of Mn–Cu based alloys," Materials Transactions, vol. 60, no. 11, pp. 2298–2304, 2019, https://doi.org/10.2320/matertrans.mt-m2019131

[17] J. Yang, et al., "Joining of Mn-Cu alloy and 430 stainless steel using Cu-based filler by SIMA-imitated brazing process," Materials Letters, vol. 253, pp. 401–404, 2019, https://doi.org/10.1016/j.matlet.2019.06.098

[18] I. B. Chudakov, et al., "Influence of plastic deformation and asymmetric loading on the properties of Fe–Al and Mn–Cu damping alloys," Steel in Translation, vol. 47, no. 6, pp. 428–433, 2017, https://doi.org/10.3103/s0967091217060031

[19] Y. Yan, S. Zhang, Y. G. Xu, et al., "A comparative study on microstructure and properties of Fe17Mn and Fe17Mn0.1C0.4Ti damping alloys under different annealing processes: Mechanics of materials," Materials Transactions, vol. 66, no. 4, 2025, https://doi.org/10.2320/matertrans.mt-m2024139

[20] F. X. Yin, et al., "EBSD characterization of the twinning microstructure in a high-damping Mn–Cu alloy," Materials Transactions, vol. 48, no. 8, pp. 2049–2055, 2007, https://doi.org/10.2320/matertrans.ma200707